

# Spectacular Shells in the Host Galaxy of the QSO MC2 1635+119<sup>1</sup>

Gabriela Canalizo<sup>2,3</sup>, Nicola Bennert<sup>3</sup>, Bruno Jungwiert<sup>3,4</sup>, Alan Stockton<sup>5</sup>, François Schweizer<sup>6</sup>, Mark Lacy<sup>7</sup>, Chien Peng<sup>8</sup>

## ABSTRACT

We present deep *HST*/ACS images and Keck spectroscopy of MC2 1635+119, a QSO hosted by a galaxy previously classified as an undisturbed elliptical. Our new images reveal dramatic shell structure indicative of a merger event in the relatively recent past. The brightest shells in the central regions of the host are distributed alternately in radius, with at least two distinct shells on one side of the nucleus and three on the other, out to a distance of  $\sim 13$  kpc. The light within the five shells comprises  $\sim 6\%$  of the total galaxy light. Lower surface brightness ripples or tails and other debris extend out to a distance of  $\sim 65$  kpc. A simple N-body model for a merger reproduces the inner shell structure and gives an estimate for the age of the merger between  $\sim 30$  Myr and  $\sim 1.7$  Gyr, depending on a range of reasonable assumptions. While the inner shell structure is suggestive of a minor merger, the total light contribution from the shells and extended structures are more indicative of a major merger. The spectrum of the host galaxy is dominated by a population of intermediate age ( $\sim 1.4$  Gyr), indicating a strong starburst episode that may have occurred at the time of the merger event. We speculate that the current QSO activity may have been triggered in the recent past by either a minor merger, or by debris from an older ( $\sim$ Gyr) major merger that is currently “raining” back into the central regions of the merger remnant.

*Subject headings:* galaxies: active – galaxies: interactions — galaxies: evolution — quasars: general — quasars: individual (MC2 1635+119)

<sup>1</sup>Based on observations made with the NASA/ESA Hubble Space Telescope, obtained at the Space Telescope Science Institute, which is operated by the Association of Universities for Research in Astronomy, Inc., under NASA contract NAS 5-26555. These observations are associated with program # GO-10421.

<sup>2</sup>Department of Physics and Astronomy, University of California, Riverside, CA 92521, USA; email: gabriela.canalizo@ucr.edu

<sup>3</sup>Institute of Geophysics and Planetary Physics, University of California, Riverside, CA 92521, USA; email: nicola.bennert@ucr.edu, bruno.jungwiert@ucr.edu

<sup>4</sup>Astronomical Institute, Academy of Sciences of the Czech Republic, Boční II 1401, 141 31 Prague 4, Czech Republic

<sup>5</sup>Institute for Astronomy, University of Hawaii, 2680 Woodlawn Drive, Honolulu, HI 96822, USA; email: stockton@ifa.hawaii.edu

<sup>6</sup>Carnegie Observatories, 813 Santa Barbara Street, Pasadena, CA 91101, USA; email: schweizer@ociw.edu

<sup>7</sup>Spitzer Science Center, California Institute of Technology, Pasadena, CA 91125, USA; email:

## 1. Introduction

The nature of QSO host galaxies has been debated for over four decades. Although the terms of the debate have gradually evolved during this time, there has been some progress. We now know, for example, that the majority of luminous low-redshift QSOs, whether radio loud or radio quiet, reside in the centers of galaxies that have relaxed light distributions like ellipticals (e.g., Disney et al. 1995; Bahcall et al. 1997; Dunlop et al. 2003; Floyd et al. 2004). This result ties in nicely with the strong correlation, determined from galaxies with inactive black holes, between supermassive black hole mass and spheroid velocity dispersion (Ferrarese & Merrit

mlacy@ipac.caltech.edu

<sup>8</sup>Space Telescope Science Institute, 3700 San Martin Drive, Baltimore, MD 21218, USA; email: cyp@stsci.edu

2000; Gebhardt et al. 2000): QSOs occur in the sorts of galaxies known to have the most massive central black holes.

At the present epoch, only a tiny fraction of galaxies with massive spheroids shows luminous QSO activity. The very steep evolution of QSO activity with redshift indicates that some additional ingredient besides the mere presence of a super-massive black hole is necessary to produce QSO activity, and that this ingredient was much more common in the early history of the Universe. It has often been speculated that the mechanism underlying this evolution is the sudden inflow of gas to the center brought about by strong interactions or mergers. There has long been a fair amount of circumstantial evidence to support this idea (see, e.g., Stockton 1999, and references therein), yet such arguments are by no means conclusive.

The debate about the nature of QSO host galaxies presently centers on the question of how significant tidal interactions are for QSOs generally: Do *most* QSOs at the current epoch begin their lives as mergers, or do most QSOs simply occur in old ellipticals to which nothing very interesting has happened recently?

We are conducting a coordinated study with Keck spectroscopy and Hubble Space Telescope (*HST*) imaging of classical QSO host galaxies to investigate whether such hosts are truly quiescent ellipticals with ancient stellar populations, or whether they are the results of mergers in the more recent past and have assumed elliptical morphologies only as a result of violent relaxation due to the mergers.

Elliptical hosts formed through mergers would be expected to show fine structure indicative of past tidal interactions, such as shells and ripples. Studies of nearby merger remnants (e.g., Schweizer & Seitzer 1992; Schweizer et al. 1990) indicate that such structure can in general be detected even a few Gyr after the last major merger event.

To look for any potential fine structure, we recently obtained very deep *HST* Advanced Camera for Surveys (ACS) images in a pilot study of five classical QSO host galaxies. In this paper, we present results for the first object, MC2 1635+119. The remaining four objects will be discussed in a subsequent paper (Bennert et al., in preparation).

The host galaxy of MC2 1635+119 ( $z = 0.146$ ;  $1'' \simeq 2520$  pc for  $\Omega_\Lambda = 0.7$ ,  $\Omega_{\text{matter}} = 0.3$ , and  $H_0 = 71 \text{ km s}^{-1} \text{ Mpc}^{-1}$ ) was first described by Hutchings et al. (1988) as having “slightly elliptical amorphous structure” with a luminosity profile that does not follow a simple exponential or  $r^{1/4}$  law. Several companions are seen in the optical images (Hutchings et al. 1988; Malkan 1984) as well as in the IR (Dunlop et al. 1993), without any clear signs of interaction (Hutchings et al. 1988). McLure et al. (1999) compare fits to the host galaxy using an exponential disk and a de Vaucouleurs spheroid model, and conclude that the host resembles more closely an elliptical. Regarding the stellar contents, Nolan et al. (2001) estimate an age of 12 Gyr for the dominant stellar population in the host galaxy from off-nuclear spectra.

Thus, previous studies seem to indicate that the galaxy hosting MC2 1635+119 is an elliptical with an old stellar population. We now present new *HST* and Keck observations that are in stark contrast with any such conclusions.

## 2. Observations and Data Reduction

Spectroscopic observations and their analysis are described in detail elsewhere (Canalizo & Stockton, in preparation). Briefly, we obtained a spectrum of the host galaxy of MC2 1635+119 with a total exposure time of 1.5 hours using the Low-Resolution Imaging Spectrometer (LRIS; Oke et al. 1995) on the Keck I telescope on 2002 March 4. We used the 400 groove  $\text{mm}^{-1}$  grism blazed at 3400 Å for the blue side (LRIS-B), and the 300 groove  $\text{mm}^{-1}$  grating blazed at 5000 Å for the red side (LRIS-R), yielding dispersions of  $1.09 \text{ Å pixel}^{-1}$  and  $2.55 \text{ Å pixel}^{-1}$  respectively. The slit was  $1''$  wide, projecting to  $\sim 7$  pixels on the UV- and blue-optimized CCD of LRIS-B and  $\sim 5$  pixels on the Tektronix 2048×2048 CCD of LRIS-R. The slit position angle (PA) was  $57^\circ$ , placed roughly along the semi-major axis of the host galaxy and going through the QSO nucleus. The object was observed near transit, so that the effects of differential atmospheric refraction were minimized.

The host galaxy spectrum was reduced using standard procedures. A scaled version of the QSO spectrum was subtracted from that of the host

galaxy; the spectrum was scaled by measuring the amount of flux in broad lines in the spectrum of the host. The final spectrum corresponds roughly to a region 2–5'' from the nucleus on either side of the QSO and has a signal-to-noise ratio  $\sim 20$ . The spectrum was then modeled by performing least-squares fits to the data using preliminary Charlot & Bruzual (2007) and Maraston (2005) population synthesis models as described in § 6. Both the models and the observed spectrum were rebinned to the same spectral resolution.

Imaging observations were obtained using ACS/WFC onboard the *HST* with the broad V-band F606W filter ( $\Delta\lambda = 2342\text{\AA}$ ; 1 pixel corresponds to 0.05''). We obtained five sets of dithered images, each with four subsets of 550–586 s exposures, yielding a total integration time of 11432 s.

We re-calibrated the data manually, starting from the pipeline flat-fielded individual exposures to improve the bias subtraction, i.e., to correct the offset (of a few DN) between the adjacent quadrants that is still present in the final product of CALACS (Pavlovsky et al. 2005). We then used MultiDrizzle (Koekemoer et al. 2002) to combine the individual images, using the default values, bits=8578, as well as a delshift-file containing the offsets between the images as determined from stars within the field-of-view (FOV). The final distortion-corrected image is shown in Fig. 1, where the host galaxy shows clear shell structure.

### 3. Image Processing

To enhance and analyze any fine structure that might be present, we applied various methods such as unsharp masking, creating a so-called structure map (Pogge & Martini 2002), as well as subtracting a central point spread function (PSF) for the QSO and a host galaxy model making use of GALFIT (Peng et al. 2002). All different approaches confirm the existence of distinctive shells in the host galaxy (Fig. 2), and we discuss each of them in turn.

To create an unsharp-masked image, we divided the final image  $f$  by the  $f$  convolved with a Gaussian function of  $\sigma = 5$  pixel ( $G$ ):

$$f_{\text{unsharp}} = \frac{f}{f \otimes G}$$

The structure map was derived by dividing  $f$  by the PSF-smoothed image ( $f \otimes P$ ) and then convolving this ratio with the transpose of the PSF ( $P^t$ ):

$$f_{\text{structure}} = \left[ \frac{f}{f \otimes P} \right] \otimes P^t$$

This process enhances unresolved or slightly resolved structures on the scale of the PSF by removing the smooth light distribution on larger scales (Pogge & Martini 2002).

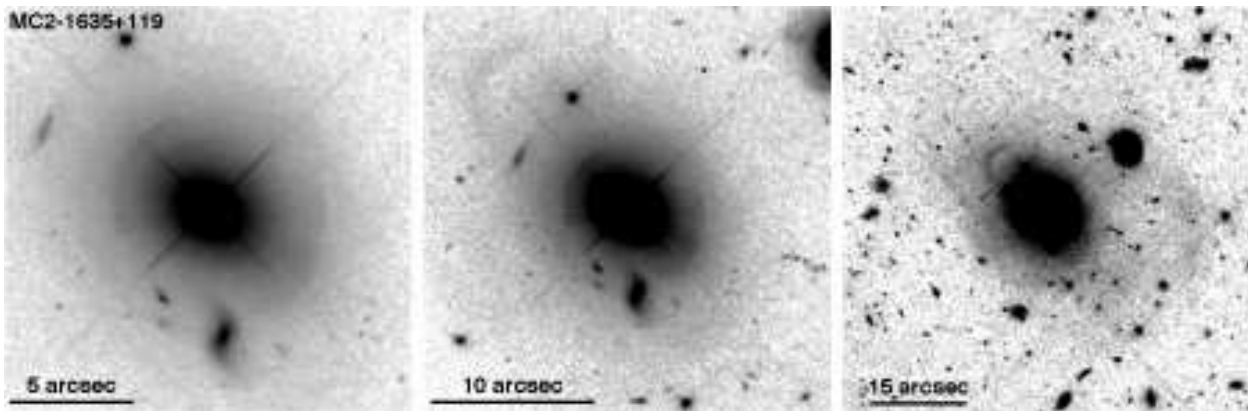


Fig. 1.— ACS/WFC image of MC2 1635+119, shown at different scales. Fine structure consisting of shells, arcs, and other debris is clearly seen at small and large scales. The images have been Gaussian smoothed with a sigma of either 0.5 pixels (left and central panels) or 2 pixels (right panel). In this and the following figures, north is up and east is to the left.

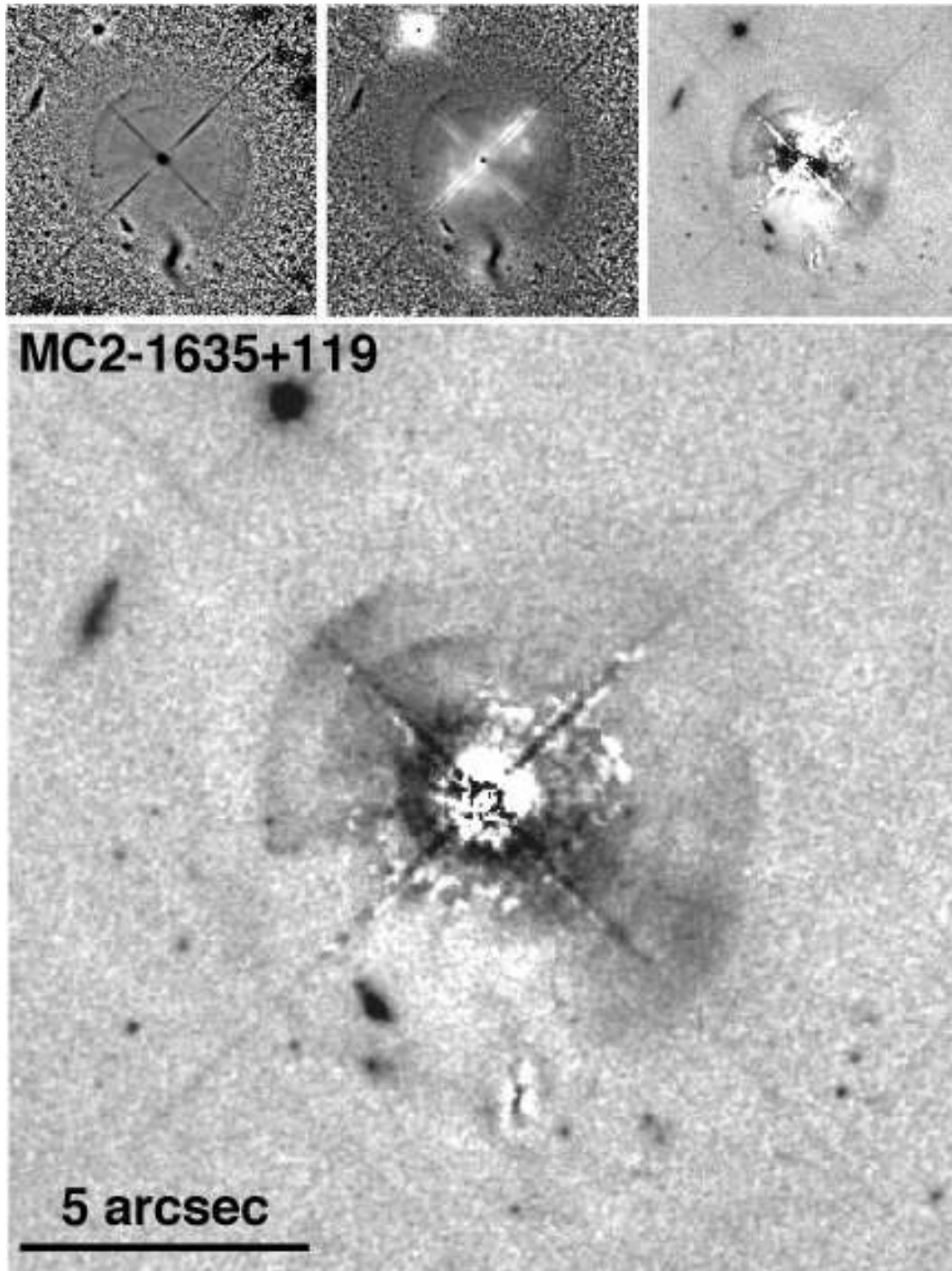


Fig. 2.— Different methods used to detect fine structure in MC2 1635+119, as described in the text. *Top left*: an unsharp-masked image,  $f_{\text{unsharp}}$ . *Top middle*: a structure map,  $f_{\text{structure}}$ . *Top right*: a residual image using GALFIT, where the model used for the host galaxy consists of a de Vaucouleurs profile only. *Bottom*: a residual image using GALFIT, where the model used for the host galaxy consists of a de Vaucouleurs and a Sérsic profile of index  $n \sim 1$ .

A PSF image is needed for both the structure map and for modeling with GALFIT. Therefore, we created an artificial PSF from TinyTim (Version 6.3) at the same position as our object as well as a “real” PSF using a star on an ACS/WFC F606W image. This image was obtained by searching the *HST* archive for a suitable star at roughly the same chip position as the QSO and with a high signal-to-noise ratio (S/N). We found a star at  $< 30$  pixels away from the position corresponding to the QSO with a S/N of 20000 that was observed on 20 dithered images with a total exposure time of  $\sim 8100$ s (GO-9433, datasets j6mf19\* and j6mf21\*). We processed these images in the same manner as described above for our data.

In order to minimize introducing additional noise into the PSF subtraction and convolution operations, we first eliminated a few faint objects surrounding the PSF. Then, depending on the data values compared to the standard deviation  $s$  of the surrounding sky, we modified the PSF image as follows: (1) for data values  $> 7s$ , we retained the unmodified PSF; (2) for data values between  $3s$  and  $7s$ , we smoothed the image with a Gaussian kernel with  $\sigma = 0.5$  pixel; (3) for smaller data values, we smoothed with a Gaussian kernel with  $\sigma = 2.0$  pixel; finally, (4) for data values that were  $< s$  after this last operation, we replaced the value with 0.

To probe the quality of the two different PSFs, we subtracted them from both saturated and unsaturated stars within our FOV using GALFIT: the real PSF star gave significantly better results than the TinyTim PSF. From this exercise, we also determined the central region with a radius of  $\sim 1''.7$  is strongly affected by the PSF subtraction because the QSO nucleus was saturated; any structure seen within this region is likely an artifact.

The best enhancement of the shell structure was obtained using GALFIT (Fig. 2), a 2-dimensional galaxy fitting program capable of fitting simultaneously one or more objects in an image with different model light distributions (such as Sérsic (1968), de Vaucouleurs (1948), exponential, etc.; Peng et al. 2002). Briefly, our adopted procedure was as follows: First, we created a mask to exclude the saturated pixels in the center, the diffraction spikes, any surrounding bright objects, and the

shells themselves, in order to fit only the smooth underlying host galaxy light distribution. Then, a (“real”) PSF as well as several Sérsic functions were fitted. In GALFIT, the Sérsic power law is defined as

$$\Sigma(r) = \Sigma_e \exp \left[ -\kappa \left( \left( \frac{r}{r_e} \right)^{1/n} - 1 \right) \right]$$

where  $\Sigma_e$  is the pixel surface brightness at the effective radius  $r_e$  (Peng et al. 2002), and  $n$  is the Sérsic index ( $n = 4$  de Vaucouleurs,  $n = 1$  exponential profile). In addition, we fitted the bright neighbor to the south of the QSO with a Sérsic function. In all steps, the background sky was fitted simultaneously. This least-squares fit was then subtracted from the original image to gain the residual image, enhancing all structure that lies on top of the smooth host galaxy light distribution.

When we used a single component for the host galaxy, the best fit was achieved with a Sérsic function of index  $n = 8.8$ . This fit was marginally better (only a few percent in  $\chi^2$ ) than the fit achieved using a de Vaucouleurs profile. On the other hand, the fit resulting from an exponential profile was much worse (roughly 50% in  $\chi^2$ ). This finding is in agreement with the results by McLure et al. (1999), who determined that the host galaxy of MC2 1635+119 is better fit by a de Vaucouleurs than an exponential profile.

The fit improved substantially, however, when two components were included instead of one. Using two Sérsic functions, the best result was achieved when one had an index  $n=4$ , which corresponds to a de Vaucouleurs profile, and the other an index  $n=0.91$ , which corresponds nearly to an exponential disk; this fit is shown in Fig. 2 and listed in Table 1. If, instead, the index of one of the Sérsic components was fixed to  $n=1$  (exponential), the best fit was achieved when the other component was close to a de Vaucouleurs profile (with index  $n=4.6$ ; Table 1). Therefore, we conclude that the host galaxy is well modeled by a de Vaucouleurs spheroid plus an exponential disk that makes up roughly one fourth of the light in the surface brightness profile, as detailed in Table 1. In that table, we also list results for the fit using a de Vaucouleurs profile only in order to compare our results with those of Dunlop et al. (2003), and we find that our results are very sim-

ilar to theirs. However, as Fig. 2 shows, the resulting model-subtracted image using only a de Vaucouleurs profile has residuals that are significantly larger than those obtained when we use a two-component model.

#### 4. Shell Structure and Luminosity

In Fig. 3 we show a residual image of MC2 1639+119 indicating the position of the different tidal features that we identify. The central circle with a radius of  $1''.7$ , corresponds to the area most affected by the saturated PSF; any features within this area may be artifacts of the PSF subtraction. Unfortunately, this prevents us from reliably detecting any shells or other structure that may be present in that region.

The arcs labeled *a* through *e* in Fig. 3 are all segments of circles centered on the galaxy, emphasizing the regularity of the interleaved shells. The projected radii of these shells are roughly 6.6, 7.6, 8.3, 10.0, and 12.5 kpc, respectively. This set of bright shells is closely aligned with the semi-major axis of the host galaxy, at PA  $\sim 54^\circ$ . The shell system shows roughly a biconical structure, although the edges of this putative bicone do not intersect

at the center of the host galaxy. Shell *e* shows a discontinuity west of the QSO that may be due to obscuration by dust, or the shell may be made of two or more components.

A set of lower surface-brightness shells or ripples (*f*, *g* and *h*) with seemingly different (greater) ellipticities are seen roughly perpendicular to the first set, both north-west and south-east of the nucleus.

Further out to the north-east, there is an arc-like feature (*i*) extending out to a projected distance of  $\sim 32$  kpc. Other faint tails or wisps are seen in that same region (*j*). Finally, a much larger, faint and diffuse feature resembling either a shell or some tidal tail (*k*) is visible  $\sim 65$  kpc west of the nucleus. While this feature is very faint, we are confident it is real, particularly as this feature is also visible in a WFPC2 archival image (GO-6776) when the image is median filtered and Gaussian smoothed.

To estimate the luminosity within the shells compared to the total luminosity of the galaxy, we created a mask that includes all the light within an annulus of inner radius of  $1''.7$  and outer radius of  $6''.8$ , but that at the same time excludes the

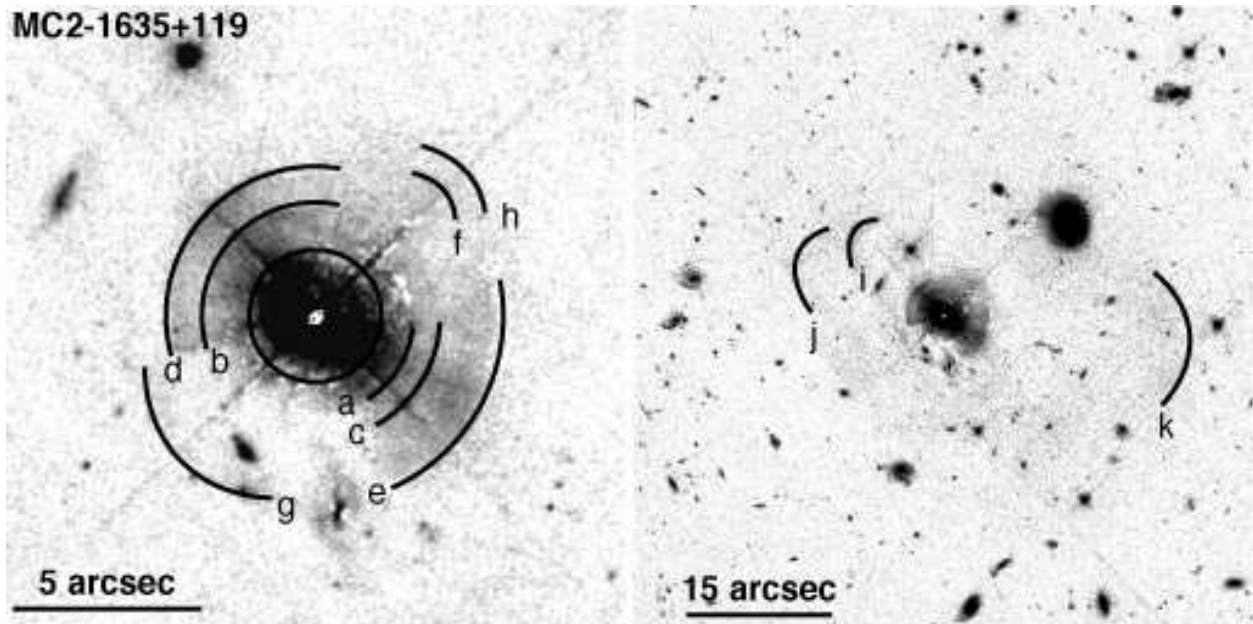


Fig. 3.— Model-subtracted images of MC2 1635+119, where the most prominent fine-structure features are labeled.

TABLE 1  
RESULTS OF MODELING THE QSO HOST GALAXY USING GALFIT

fit type (1)	function (2)	$\Delta(\alpha, \delta)$ (arcsec) (3)	$m_{F606W}$ (mag) (4)	$r_e$ (kpc) (5)	Sérsic index (6)	$b/a$ (7)	PA (deg) (8)
de Vauc+Sérsic	S1	(−0.03,0.04)	17.46	2.74	4 (fixed)	0.74	57.3
	S2	(0.72,0.26)	18.80	15.89	0.91 (free)	0.79	28.8
Sérsic+Exp	S1	(−0.03,0.04)	17.39	2.75	4.6 (free)	0.75	57.3
	S2	(0.85,0.29)	18.83	16.5	1 (fixed)	0.79	26.9
de Vauc+Exp	S1	(−0.03,0.04)	17.45	2.68	4 (fixed)	0.74	57.4
	S2	(0.72,0.26)	18.71	16.03	1 (fixed)	0.8	29.3
de Vauc only	S1	(−0.03,0.04)	17.26	5.74	4 (fixed)	0.75	52.3
Dunlop et al. (2003)	S1	...	...	5.73	4 (fixed)	0.69	56

NOTE.—Column (1) lists the GALFIT model, (2) the individual components used (S = Sérsic), (3) the offsets with respect to the PSF, (4) the integrated apparent magnitude in the F606W filter, (5) the effective radius, (6) the Sérsic index, (7) the axis ratio, and (8) the position angle (east of north). Results from Dunlop et al. (2003) are listed for comparison. Note that the PA given here for the Dunlop et al. (2003) results was derived by adding the orientation of the spacecraft to the PA given in their Table 3, which was apparently not corrected for this orientation.

diffraction spikes as well as several additional light sources from apparent companions. Note that the outer radius was chosen to be  $3 \times r_{\text{eff}}$  with  $r_{\text{eff}}$  determined from a single de Vaucouleurs fit (see Table 1). This mask (good=1, bad=0) was multiplied by the image and the total counts in the product were summed. This was done for both the GALFIT residual image ( $f_{\text{shells}}$ ) obtained subtracting the GALFIT model of a de Vaucouleurs + exponential profile, and the GALFIT model itself ( $f_{\text{galaxy}}$ ). Finally, we computed the ratio  $f_{\text{shells}}/f_{\text{galaxy}}$ . This yields the fractional luminosity of the shells between 1''7 and 6''8 radius as  $\sim 6\%$  of the host galaxy light (within the same annulus). This estimated percentage may be smaller or larger than the true percentage depending on whether there are any shells within the radius affected by the PSF subtraction or not.

Note that the percentage given refers to the total flux within the shells out to 13 kpc. However, the local contrast between the shells and the galaxy (as estimated by dividing the residual image by the GALFIT model) varies between 5 and 20% and reaches 50% in Shell *e*.

## 5. Time Constraints from Tidal Structure

As described above, the host galaxy of MC2 1635+119 reveals spectacular structure of regular and aligned shells on projected radii of 5-13

kpc. Similar shells are observed in some local giant ellipticals (e.g., Malin & Carter 1983; Schweizer 1980; Sikkema et al. 2007) and are interpreted as remnants of a merger event. It has been shown that the mergers that produce shell-like structure can be either minor (Quinn 1984, hereafter Q84) or major (e.g., Hernquist & Spergel 1992). In this section, we discuss both scenarios in the context of the morphology and physical size of the shells and structure we detect, with the aim of placing constraints on the age of the tidal interaction that formed them.

### 5.1. Minor Merger

We first consider the case of a minor merger since it allows for the simplest physical interpretation of the data. In this scenario, the system of regular concentric shells, confined within a finite range in azimuth, can result from the merger of a smaller galaxy (either spiral or elliptical) with a large elliptical along a nearly radial orbit (Q84; Dupraz & Combes 1986; Hernquist & Quinn 1988, 1989, hereafter HQ88 and HQ89).

The shell formation mechanism works as follows: during the merger, stars from the smaller galaxy are captured by the massive galaxy and start to oscillate in its potential well. Since stars spend most of the time near the apocenters of their

orbits (where their radial velocities go to zero), a relative enhancement of the stellar density (a shell) forms there. The first shell is formed by captured stars that were initially in orbits with the smallest oscillation period, i.e., those with the smallest apocenter distance.

As time goes on, the shortest-period stars move away from apocenter, while stars with slightly longer periods reach their apocenter at a slightly larger galactocentric distance. Due to a continuous range of oscillation periods, the first shell appears to propagate radially outward while its stellar content progressively changes: it is thus a radially propagating stellar density wave. A new traveling shell appears every time the shortest-period stars complete another oscillation period. After several oscillations, the massive elliptical galaxy reveals a system of shells where the outermost shell is the oldest, since this is the shell that formed first. This scenario gives a simple relation between the radius of this shell and the time of its formation.

We have constructed a simple N-body model that reproduces, at least qualitatively, the brightest shells observed in MC2 1635+119. The N-body model uses the same technique as that used by Q84 and HQ88. In this model, the secondary (smaller galaxy) moves on a radial orbit and is assumed to be disrupted instantaneously by the tidal forces of the primary (massive elliptical) after the first passage through the center of the primary. This corresponds to abruptly lowering the secondary’s mass to zero, after which the test particles move in the potential of the primary alone. Thus, dynamical friction is assumed to be unimportant, and the model should only be considered as a zero-order description of the collision.

We assumed a radial orbit with an initial separation between galaxies arbitrarily chosen to be 90 kpc (5-18 times the scale-length of the primary). The initial infall velocity of the secondary was set equal to the escape velocity for the potential of the primary.

We simulated the merger using (1) a de Vaucouleurs profile, and (2) a Plummer sphere (corresponding to a Moffat’s  $n=2$  surface brightness profile). Since the goal of these simulations was to provide only a first order estimate of the merger timescale, we did not attempt to use more realistic composite density profiles of luminous and dark

matter. We used effective radii ranging from 5 to 20 kpc; this range spans values for  $r_{\text{eff}}$  found by Dunlop et al. (2003), Taylor et al. (1996), and our own work (all corrected to the cosmology used in this paper). The mass of the giant elliptical was taken to be  $3.2 \times 10^{11} M_{\odot}$  (Dunlop et al. 2003), although we allowed for a range of masses up to  $3.2 \times 10^{12} M_{\odot}$  in order to account for a dark matter halo. The secondary-to-primary mass ratio and scale-length ratio were both fixed to 0.1; we note that while the precise choice of these two ratios is arbitrary, they affect mainly the contrast of the shells, and not the timescales, as long as the primary dominates the potential.

Figure 4 shows our results for simulations using a Plummer surface brightness profile. The de Vaucouleurs model, which leads to lower contrast and more spherical shells, will be discussed in more detail in a subsequent paper (Jungwiert et al., in preparation). Table 2 lists the timescales for two outermost shells (see below) to reach their observed radii in models with the range of parameters for the primary given above. We measure this timescale from the moment when the centers of mass of the two galaxies pass by each other (hereafter “merger timescale”). We do not attempt to use the sizes or separations of inner shells to constrain the timescale since inner shells are more sensitive to the exact shape of the central density profile of the primary and are also more likely to be influenced by dynamical friction, which is not implemented in our model.

Table 2 shows that, allowing for an uncertainty in the type of profile, for a rather large uncertainty in the effective radius, and for a considerable amount of dark matter, the time for Shell *e* to reach its present distance of 12.5 kpc appears to be confined to a range of  $\sim 30$ –400 Myr after the centers of the two galaxies passed through each other.

These ages are calculated assuming that Shell *e* is the outermost shell. However, we might consider the possibility that the tidal feature *k* may be a much older, fainter shell formed during the same encounter. This “shell”, at a projected distance of  $\sim 65$  kpc from the center of the host galaxy, would then give a merger timescale ranging from 100 Myr to 1.7 Gyr (see Table 2), given the assumptions considered above.

We emphasize that our simulations model the



TABLE 2  
SHELL FORMATION TIMESCALES FROM NUMERICAL SIMULATIONS

$R_{shell}$ (kpc)	$M_{primary}$ ( $M_{\odot}$ )	$T_{deVauc}$ (Myr)	$T_{Plummer}$ (Myr)
12.5	$3.2 \times 10^{11}$	100 – 245	145 – 400
	$3.2 \times 10^{12}$	30 – 60	45 – 135
65	$3.2 \times 10^{11}$	360 – 1720	1380 – 1620
	$3.2 \times 10^{12}$	100 – 400	440 – 510

NOTE.—The time range given for each model corresponds to a range of effective radii for the giant elliptical of 5 to 20 kpc. The time is measured from the moment when the centers of mass of the two galaxies pass through each other.

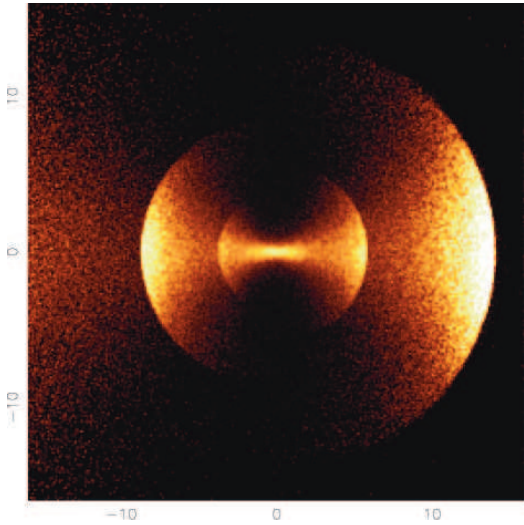


Fig. 4.— Shell structure in a restricted N-body simulation of a minor merger of two ellipticals (gE+dE). The masses of the galaxies are, respectively,  $3.2 \times 10^{11} M_{\odot}$  and  $3.2 \times 10^{10} M_{\odot}$ , and their effective radii 5 and 0.5 kpc. Both galaxies are modeled as Plummer spheres. The smaller galaxy came from the right on a radial orbit. The box is  $16 \times 16$  kpc. Only the particles belonging to the smaller galaxy are shown, to allow for comparison with images where a model of the host galaxy has been subtracted.

simplest plausible case, and at this point we cannot exclude more complicated scenarios. In a subsequent paper (Jungwiert et al., in preparation) we will consider N-body simulations of this galaxy and of shell galaxies in general in more detail, focusing on different gravitational potentials, various mass ratios of colliding galaxies, dynamical friction, tidal stripping and the fate of gas.

## 5.2. Major Merger

While the numerical simulations described above can reproduce the morphology of the brightest shells in MC2 1635+119, they do not rule out the possibility that the shells might have been created by a major merger. Further, the model-subtracted images (Figs. 2 and 3) show features ( $f$ ,  $g$ ,  $h$ ) that are off-axis from the direction of the encounter implied by the inner shells. Additional tidal debris at different position angles is seen on much larger scales (features  $i$ ,  $j$ ,  $k$ ). It is difficult to explain how all this structure might have formed as a result of a minor merger, provided a single interaction is responsible for all the features.

The fact that the inner shells appear to be closely aligned with the major axis of the host would also argue against a minor merger (see Hernquist & Spergel 1992, and references therein). Using numerical simulations, Hernquist & Spergel (1992) show that mergers between two disk galax-

ies of similar mass can form shells, loops, and ripples. In particular, their simulations are compared to NGC 3923, one of the best examples of a nearby elliptical galaxy with shells (Malin & Carter 1983). The system of shells of NGC 3923 ( $z = 0.005801$ ) extends from distances close to the center ( $< 2$  kpc) out to  $\simeq 100$  kpc (Priour 1988). The shells are distributed roughly in an hour-glass shape with an opening angle of  $\simeq 60^\circ$ . While most of the shells appear aligned with the major axis of the galaxy, the outermost shell does not, a feature that is nicely reproduced by the simulations by Hernquist and Spergel. These characteristics are similar to those observed in MC2 1635+119, although it should be noted that the structure of the inner shells in MC2 1635+119 is significantly more regular (non-intersecting and aligned) than that of the NGC 3923 shells or of the numerical simulations by Hernquist & Spergel (1992). However, the comparison does point out that a major merger could also have formed the shells seen in MC2 1635+119.

The amount of light observed in the shells may yield further clues to the nature of the merger. As mentioned in §4, the system of five bright shells comprises  $\sim 6\%$  of the total luminosity of the galaxy. However, the shells contain only a fraction of the total number of stars that were originally part of the merging galaxy, i.e., those whose orbital velocities are near zero. Our numerical simulations and those of Hernquist & Spergel (1992) indicate that the stars in shells make up only one fourth or less of the total mass of the companion. Therefore, assuming that the mass-to-light ratio is similar in both galaxies, the intruder may make up about 24% of the total mass. If we add to that the mass implied by the more extended “shell”, the fraction may be closer to 30%. Thus, by this argument alone, the mass ratio of the original galaxies may have been close to 7:3 which may be considered a borderline major merger.

Our simple N-body model produces shells up to a mass ratio of 3:1 for the parent galaxies. We did not investigate smaller mass ratios due to the increased complexity of such encounters. If we assume that the “shell” at 65 kpc (Shell  $k$ ) formed through a similar mechanism as that outlined in §5.1, then the range of timescales of 100 Myr to 1.7 Gyr would still hold for a major merger. If, however, this feature was formed through the spatial

wrapping of, e.g., a tidal tail, then estimating a timescale becomes more complex since timescales become more heavily dependent on initial conditions. As a reference, we note that simulations of the major merger in “The Mice” by Barnes (2004) produce a merger remnant somewhat similar to MC2 1635+119 at a time close to 1 Gyr from the beginning of the merger event.

## 6. Stellar Populations

Figure 5 shows the Keck LRIS spectrum of the host galaxy of MC2 1635+119 in rest frame, representing its integrated light from  $2''$  to  $5''$  radius along the slit on either side of the nucleus (see §2). Since the slit was placed roughly in the direction of the major axis of the host galaxy, the spectrum includes the brightest shells in the host (Fig. 3,  $a$  through  $e$ ).

The stellar component has a redshift  $z_{\text{abs}} = 0.1474$  (measured from absorption lines), equal to the redshift we measure from narrow emission lines, but slightly higher than that of the broad emission lines ( $z \sim 0.146$ ).

In order to model the spectrum, we used population synthesis models by Maraston (2005) and the preliminary models by Charlot & Bruzual (2007). We chose these two sets of models be-

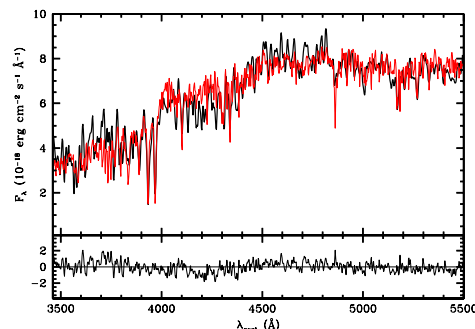


Fig. 5.— Keck LRIS spectrum of the host galaxy of MC2 1635+119 in rest frame. The black trace is the observed spectrum. The red trace is the best fit Charlot & Bruzual (2007) model to the data. The model consists of 52% (by mass) of a 1.4 Gyr old population and 48% of a 12 Gyr population. In the bottom panel we show the residuals obtained by subtracting the model from the observed spectrum.

cause they provide the best match to our spectral resolution and they both include contributions from thermally pulsating asymptotic giant branch stars, which are known to be particularly important in intermediate-age ( $\sim 1$  Gyr) stellar populations (Maraston 2005). Our original approach to analyzing the spectrum was to assume a dominant old stellar population ( $\sim 12$  Gyr) representing the population of the giant elliptical galaxy, with a smaller fraction of more recent star formation possibly triggered by the merger that formed the shells. Models that include a very small fraction ( $< 0.3\%$ ) of a young ( $< 50$  Myr) starburst and a dominant ancient population can produce a rough fit to the continuum, but the fit to individual features such as CaII H&K and the CN band is rather poor. We tested spectral fits using different metallicities ranging from 0.02 to 2 solar, and found that solar metallicity models consistently yielded the lowest  $\chi^2$ . The choice of initial mass function (Chabrier 2003; Kroupa 2001; Salpeter 1955) made little or no difference.

However, the best fit to the observed spectrum, including both the continuum and stellar features, was achieved by adding a large contribution from an intermediate-age starburst population to the 12 Gyr model. A better fit was achieved with Charlot & Bruzual (2007) than with Maraston (2005) models, but both sets of models yielded similar results. In the case of Charlot & Bruzual (2007) models, the best fit (shown in Fig. 5) corresponds to an intermediate-age population of 1.4 Gyr contributing 52% of the total mass along the line of sight. The best fit using Maraston (2005) models is for an intermediate-age population of 1.0 Gyr contributing 45% of the total mass along the line of sight. The real difference between the two models may be even smaller, considering that the Maraston models provide a coarser age grid (with steps in age at 1.0 and 1.5 Gyr) than the Charlot & Bruzual models and the fact that the  $\chi^2$  for the latter shows a shallow minimum from  $\sim 1.2$  to 1.9 Gyr (although the mass contribution from the starburst increases steeply with age). In both cases,  $\chi^2$  increases rapidly beyond 2.0 Gyr.

The determination of these intermediate-age components is robust with respect to the choice of the model for the older population: the same intermediate-age populations are obtained when the older population is varied from 6 to 14 Gyr.

If we use models of metallicities lower than solar, a single population can be used to fit the data, although the overall fit is significantly worse. In this case, the oldest population that yields a reasonable fit is less than 3 Gyr old. Single populations older than 4 Gyr yield poor fits regardless of their metallicity or initial mass function. Although it is possible that the spectrum may be somewhat reddened by dust, it is unlikely that the age of the starburst component would be significantly younger than one Gyr, given the absorption features that we observe. Finally, an inaccurate subtraction of the QSO contribution could affect the shape of the continuum. We tested the effects of this by fitting spectra that were slightly over-subtracted and under-subtracted. While the  $\chi^2$  for these cases was somewhat larger, the age of the starburst for the best fit remained the same.

Naturally, the number of possible combinations of populations to model the spectrum of the host is large. We have kept our analysis simple by testing only a limited number of possibilities corresponding to physically plausible scenarios. Therefore, while we cannot exclude more complex star-formation histories, we are fairly certain that: (1) The dominant component of the stellar population in the host of MC2 1635+119 is *not* ancient, and (2) A small percentage by mass of recent (less than a few hundred Myr) star formation superposed on an old ( $> 6$  Gyr) population can be ruled out, regardless of the age of the dominant population. Instead, the spectrum of the host of MC2 1635+119 is dominated (at least in flux) by an intermediate age population of 1–2 Gyr.

## 7. Discussion

In agreement with previous observations, we have found that the surface brightness profile of the galaxy hosting MC2 1635+119 is closer to a de Vaucouleurs than an exponential profile. However, our new ACS image reveals that a fainter exponential profile is also present, comprising up to one forth of the total luminosity. Moreover, our observations have uncovered a spectacular system of shells and other faint structure in the host galaxy at small and large scales, showing that the host is far from being undisturbed. We have also found that the stellar populations in the host galaxy seem to have a substantial contribution ( $\sim 50\%$

by mass) of an intermediate-age stellar population from a 1–2 Gyr old starburst.

While the large contribution of an intermediate-age population to the spectrum of the host galaxy of MC2 1635+119 is intriguing, it is by no means unusual. Recent studies of AGN host galaxies (e.g., Jahnke et al. 2004; Sanchez et al. 2004; Kauffmann et al. 2003; Canalizo et al. 2006) indicate that galaxies hosting the most luminous AGN are often dominated by bulges whose colors are significantly bluer than those of inactive elliptical galaxies and are consistent with the presence of intermediate-age starbursts. Based on positions of the hosts in the  $D_n(4000)/H\delta_A$  plane, Kauffmann et al. (2003) suggest that these AGN hosts have had significant bursts of star formation in the past 1–2 Gyr.

Why do AGN host galaxies show these strong intermediate-age populations? And, what is the physical connection, if any, between the putative  $\sim$ Gyr old starburst and the nuclear activity? Understanding the nature of this relation is important because it could have implications for the triggering mechanisms and duty cycles of AGN. Our study of MC2 1635+119 provides some clues that may be applicable to a larger population.

We now know that the host galaxy of MC2 1635+119 was unequivocally involved in a tidal encounter. Our rough estimates discussed in § 5 place the timescale for this encounter at less than  $\sim 1.7$  Gyr, which could be compatible with the age of the major starburst. However, the large uncertainty in our estimate does not rule out the possibility of a substantially more recent event. We are also unable to discriminate between a major and a minor merger as the culprit for the shell structure that we observe. Our results give us enough information, however, to speculate on a couple of likely scenarios.

First, consider the case where the inner shell structure was formed through the accretion of a low-mass companion (one tenth or less of the mass of the primary). The overall morphology that we observe would have to be caused by more than one event, and the fact that there was a dramatic episode of star formation more than one Gyr ago would argue for a past (major?) merger connected to the large-scale tidal debris. In that case, it is possible that the giant elliptical possessed a higher gas content as a result of the past

merger event, and so the QSO activity was more readily triggered (or rejuvenated) in it by a minor merger than it would have been in a gas-poor elliptical would. This may well be the case in Cygnus A, where an ongoing minor merger appears to be responsible for triggering the nuclear activity (Canalizo et al. 2003).

Consider now the alternative case where a major merger is responsible for both the starburst and all of the structure that we observe. This merger event would have occurred over one Gyr ago and would have likely (though not necessarily) triggered a first episode of accretion onto the black hole(s). Feedback from the QSO quenched any further star formation. Assuming theoretical estimates for the duration of QSO activity are correct (e.g.,  $10^7 - 10^8$  yr; Yu & Tremaine 2002), the QSO activity would have ceased as the merger continued its course and the morphology of the newly merged galaxies began to relax into the shape of an elliptical. Eventually, the extended tidal debris would “rain” back into the central regions of the galaxy, triggering a new episode of QSO activity. A time delay in the onset of QSO activity would be in agreement with predictions by hydrodynamical simulations of merging galaxies (see e.g., Barnes 1998; Springel et al. 2005; Hopkins et al. 2007). These models frequently predict a second peak in star formation that also occurs much later in the merger. Since our spectroscopic observations exclude a radius of  $\sim 5$  kpc around the nucleus, we would not have detected any recent star formation that may be present in the central regions of the host galaxy.

While these are interesting scenarios, they are, for the moment, no more than “guided” speculation. More complete N-body models as well as high angular-resolution spectroscopy to measure the kinematics of the stellar component are needed to get a better handle on the kind of encounter that formed the observed structure. However, we will also need to study larger samples to attempt to answer more complex questions, such as the precise timing of the triggering of the QSO activity, which in turn should help answer questions regarding duty cycles and feedback.

We thank S. Charlot and G. Bruzual for providing access to their models prior to publication and the referee for helpful comments. Support

for Program # GO-10421 was provided by NASA through a grant from the Space Telescope Science Institute, which is operated by the Association of Universities for Research in Astronomy, Incorporated, under NASA contract NAS5-26555. Additional support was provided by the National Science Foundation, under grant number AST 0507450. B.J. acknowledges support by the Grant No. LC06014 of the Czech Ministry of Education and by the Research Plan No. AV0Z10030501 of the Academy of Sciences of the Czech Republic. Some of the data presented herein were obtained at the W.M. Keck Observatory, which is operated as a scientific partnership among the California Institute of Technology, the University of California and the National Aeronautics and Space Administration. The Observatory was made possible by the generous financial support of the W.M. Keck Foundation. The authors wish to recognize and acknowledge the very significant cultural role and reverence that the summit of Mauna Kea has always had within the indigenous Hawaiian community. We are most fortunate to have the opportunity to conduct observations from this mountain.

*Facilities:* HST (ACS), Keck:I (LRIS)

## REFERENCES

- Bahcall, J., Kirhakos, S., Saxe, D. H., Schneider, D. P. 1997, *ApJ*, 479, 642
- Barnes, J.E. 1998, in *Galaxies: Interactions and Induced Star Formation*, ed. D. Friedli, L. Martinet, & D. Pfenniger (Berlin: Springer), 275
- Barnes, J.E. 2004, *MNRAS*, 350, 798
- Canalizo, G., Max, C., Whysong, D., Antonucci, R., Dahm, S.E. 2003, *ApJ*, 597, 823
- Canalizo, G., Stockton, A., Brotherton, M. S., Lacy, M. 2006, *NewAR*, 50, 650
- Chabrier, G. 2003, *PASP*, 115, 763
- Charlot, S., Bruzual, A. G. 2007, *MNRAS*, in preparation
- de Vaucouleurs, G. 1948, *Ann. d’Astrophys.*, 11, 247
- Disney, M. J., et al. 1995, *Nature*, 376, 150
- Dunlop, J. S., Taylor, G. L., Hughes, D. H., Robson, E. I. 1993, *MNRAS*, 264, 455
- Dunlop, J. S., McLure, R. J., Kukula, M. J., Baum, S. A., O’Dea, C. P., Hughes, D. H. 2003, *MNRAS*, 340, 1095
- Dupraz, C., Combes, F. 1986, *A&A*, 166, 53
- Dupraz C., Combes, F., 1987, *A&A* 185, L1
- Ferrarese, L., Merritt, D. 2000, *ApJ*, 539, L9
- Floyd, D.J.E., Kukula, M.J., Dunlop, J.S., McLure, R.J., Miller, L., Percival, W.J., Baum, S.A., O’Dea, C.P. 2004, *MNRAS*, 355, 196
- Gebhardt, K., et al. 2000, *ApJ*, 539, L13
- Grogin, N. A., et al. 2005, *ApJ*, 627, L97
- Hernquist, L., Quinn, P.J. 1988, *ApJ*, 331, 682
- Hernquist, L., Quinn, P.J. 1989, *ApJ*, 342, 1
- Hernquist, L., Spergel D. N. 1992, *ApJ*, 399, L117
- Hopkins, P.F., Hernquist, L., Cox, T.J., Keres, D. 2007, submitted to *ApJ*, arXiv:0706.1234v1
- Hutchings, J. B., Johnson, I., Pyke, R. 1988, *ApJS*, 66, 361
- Jahnke, K., Kuhlbrodt, B., Wisotzki, L. 2004, *MNRAS*, 352, 399
- Kauffmann, G., et al. 2003, *MNRAS*, 346, 1055
- Kroupa, P., 2001, *MNRAS*, 322, 231
- Koekemoer A. M., Fruchter, A. S., Hook, R. N., Hack, W. 2002, *HST Calibration Workshop*, p. 337
- Malin, D.F., Carter, D. 1983, *ApJ*, 274, 534
- Malkan, M. A. 1984, *ApJ*, 287, 555
- Maraston, C. 2005, *MNRAS*, 362, 799
- McLure, R. J., Kukula, M. J., Dunlop, J. S., Baum, S. A., O’Dea, C. P., Hughes, D. H. 1999, *MNRAS*, 308, 377
- McLure, R. J., Dunlop, J. S. 2001, *MNRAS*, 327, 199
- Nolan, L. A., Dunlop, J. S., Kukula, M. J., Hughes, D. H., Boroson, T., Jimenez, R. 2001, *MNRAS*, 323, 308

- Oke, J. B., et al. 1995, *PASP*, 107, 375
- Pavlovsky, C., et al. 2005, "ACS Data Handbook",  
Version 4.0, (Baltimore: STScI)
- Peng, C. Y., Ho, L. C., Impey, C. D., Rix, H.-W.  
2002, *AJ*, 124, 266
- Pierce, C.M., et al. 2007, *AJ*, 660, L19
- Pogge, R. W., Martini, P. 2002, *ApJ*, 569, 640
- Prieur, J.-L. 1988, *ApJ*, 326, 596
- Quinn, P.J. 1984, *ApJ*, 279, 596
- Salpeter, E.E., 1955, *ApJ*, 121, 161
- Sanchez, S. F., et al. 2004, *ApJ*, 614, 586
- Schweizer, F. 1980, *ApJ*, 237, 303
- Schweizer, F., Seitzer, P. 1992, *AJ*, 104, 1039
- Schweizer, F., Seitzer, P., Faber, S. M., Burstein,  
D., Dalle Ore, C. M., Gonzalez, J. J. 1990, *ApJ*,  
364, L33
- Sérsic, J. L. 1968, *Atlas de Galaxias Australes*  
(Córdoba: Obs. Astron., Univ. Nac. Córdoba)
- Sikkema, G., Carter, D., Peletier, R.F., Balcells,  
M., del Burgo, C., Valentijn, E.A. 2007, *A&A*,  
467, 1011
- Springel, V., Di Matteo, T., Hernquist, L. 2005,  
*MNRAS*, 361, 776
- Stockton, A. 1999, in *Galaxy Interactions at Low  
and High Redshift*, IAU Symp. 186, eds. D.  
Sanders & J. Barnes (San Francisco: Astron.  
Soc. Pac.), p. 311
- Taylor, G. L., Dunlop, J. S., Hughes, D. H., Rob-  
son, E. I. 1996, *MNRAS*, 283, 930
- Yu, Q., Tremaine, S. 2002, *MNRAS*, 335, 96
- Wu, X.-B., Liu, F. K., Zhang, T. Z. 2002, *A&A*,  
389, 742